

We are IntechOpen, the world's leading publisher of Open Access books Built by scientists, for scientists

6,100

Open access books available

149,000

International authors and editors

185M

Downloads

Our authors are among the

154

Countries delivered to

TOP 1%

most cited scientists

12.2%

Contributors from top 500 universities



WEB OF SCIENCE™

Selection of our books indexed in the Book Citation Index
in Web of Science™ Core Collection (BKCI)

Interested in publishing with us?
Contact book.department@intechopen.com

Numbers displayed above are based on latest data collected.
For more information visit www.intechopen.com



Chapter

Aged Biochar for the Remediation of Heavy Metal Contaminated Soil: Analysis through an Experimental Case the Physicochemical Property Changes of Field Aging Biochar and Its Effects on the Immobilization Mechanism for Heavy Metal

Run-Hua Zhang, Lin-Fang Shi, Zhi-Guo Li, Guo-Lin Zhou, Yan-Lan Xie, Xing-Xue Huang, An-Hua Ye and Chu-Fa Lin

Abstract

Heavy metal inducing contamination soil has become a serious concern. Contaminated soil can cause physiochemical and biochemical changes into soil and the plants. Thus, the plant growth and the yield were affected. In additionally, that ultimately leads to the problem of food security and human health. In recent years, many kinds of ways were used for the remediation of heavy metal contaminated soil, such as isolation, phytoremediation, immobilization, extraction, and soil washing. As a new carbon-rich material, biochar has been applied to the remediation of heavy metal pollution in soil. As biochar is rich with porous structure, high cation exchange capacity, pH value, and surface function, it has become an adsorbent for soil heavy metal remediation. While, with time, the capacity of biochar to immobilize the heavy metals may be modified as the sorption sites may get occupied with native soil organic matter or competing contaminant, etc. And that the physicochemical properties of biochar changed significantly during field aging. Thus, to clarify the mechanism of field-aged biochar for the remediation of heavy metal contaminated soil, we analysis, through an experimental case, the physicochemical property changes of field-aged biochar and its effects on the immobilization mechanism for heavy metal.

Keywords: field-aged biochar, heavy metal, contaminated soil, remediation, adsorption mechanism

1. Introduction

Heavy metal pollution such as cadmium (Cd), lead (Pb), arsenic (As), and chromium (Cr) is characterized by high toxicity and biological enrichment in soil. Heavy metal contamination in soil poses a potential threat to human health and food security [1–3]. In addition, different types and concentrations of heavy metals often exist at the same time, making the polluted soil environment more complex. Therefore, it is urgent to seek remediation technology to remove heavy metals from contaminated soil. Fortunately, biochar, as an economical and efficient adsorption material, has opened up a new way for the immobilization of heavy metals [4, 5].

Biochar is an organic and pyrogenic material produced by pyrolysis of animal or plant-based feedstocks under oxygen limited conditions [6, 7]. In the pyrolysis process, the fatty carbon chain (c) in the raw material finally forms aromatic C, which is considered as fixed C and can exist in the soil for hundreds or thousands of years. The intermediate products between the fixed C surfaces are called active components. When biochar was applied to the soil, they are easily decomposed or weathered and oxidized by soil microorganisms, thus reducing the content of biochar in the soil.

At the present time, increasingly studies show that the properties of biochar will change significantly due to the influence of various environmental factors. This was identified as biochar field aging [8–10]. As far as we know, biochar mainly fixes heavy metals in soil or water through precipitation, surface complexation, cation exchange, electrostatic attraction, and cation- π interaction [11]. However, the field aging of biochar will cause the interaction between biochar and organic matter, minerals, and dissolved organic matter in soil [12]. These resulted in the change of specific surface area (SSA), cation exchange capacity (CEC), element composition, acidity, and O-containing functional group of biochar. These will further affect the ability to absorb heavy metals of biochar and its field application performance. The research showed that most biochar increased the content of O-containing functional groups after biochar artificial aging and enhanced the adsorption capacity of heavy metal [13]. However, Lin reported that water washing aging biochar and acidification treatment had a negative impact on the biochar's aluminum toxicity reduction and the improvement of acidic soil [14]. These contradictory results can be explained by many factors. To sum up, there is no consensus on whether the adsorption capacity of biochar for heavy metals changes with biochar field aging and how it changes with field aging.

Although the related research on the aging of biochar is booming, most of the research of the biochar aging is carried out by the simulated aging method under the controllable laboratory conditions [15]. It is not under the field conditions. Actually, there are great differences between artificial aging and field aging of biochar. That is, the changes of physical and chemical properties of biochar under field aging are different from under the artificial aging. So far, there are few studies on the characterization of physical and chemical properties of aged biochar (ABC) extracted from soil [16, 17]. Not to mention the influence of physical and chemical properties of field-aged biochar on heavy metal adsorption. Therefore, we studied the characteristics of field-aged biochar for the remediation of heavy metal contaminated soil by analysis through an experimental case the physicochemical property changes of field aging biochar and its effects on the immobilization mechanism for heavy metal.

2. Biochar

2.1 Preparation of biochar

Biochar is carbon-rich byproduct of pyrolyzing material (feedstocks) at high temperatures and low oxygen levels. It has porous structure, larger surface area, ample surface functional groups, and good CEC [17]. These unique physiochemical properties and distinct role of biochar give it to improve the soil biological and physiochemical properties, carbon sequestration, and remediation of heavy metals in soil. Biochar's physical and chemical residences rely on the categories of feedstocks and pyrolysis situations.

The feedstocks of biochar can classify into virgin sources, residues, and municipal solid wastes. The virgin sources include forest sources and oilseed/cereal crops. The residues are timber residues, agricultural residues, and wastes of livestock residues [18]. The wood, wood pellets, tea trash, coffee hulls, biodegradable sewage sludge, wheat straw, rice straw, macro and microalgae, maize fodder are unquestionable fantastic potentials as pyrolysis feedstocks so far.

Up to now, the pyrolysis situations of biochar are conventional pyrolysis, microwave-assisted pyrolysis, impregnation pyrolysis, co-precipitation, hydrothermal carbonization, etc. The conventional pyrolysis is the standard heating system in which heat is transferred from an external supply to the biomass through conductivity, radiation, and convection. It is inefficient and slow and dependent on the biomass thermal conductivity as well as the system's convection present day [17]. Microwave-assisted pyrolysis entails strength conversion rather than mere heating. At some point of this approach, electromagnetic energy is regenerated into thermal energy by using dielectric heating. And the temperature of the feedstock at its center is higher than the temperature of the components. This system accelerates chemical reactions and shortens their duration, saving energy surface and time [18]. This approach is among the foremost promising strategies of fast and improving chemical reactions. The magnetic biochar was obtained from the impregnation-pyrolysis system. It has been studied and used extensively at present. Firstly, the biomass was impregnated in a solution that has transition metal salt and without the solvent. Then the dried residue is pyrolyzed in inert or anoxic atmosphere to get the magnetic biochar [19]. The synthesis of magnetic biochar by co-precipitation was more sophisticated than the impregnation-pyrolysis methodology. However, it is more manageable, allowing the magnetic medium to be stably adhered to the biochar matrix. In co-precipitation system, the biochar was firstly dispersed into a solution containing transition metals with the pH range of 9–11 for a while at a given temperature. And then, the supernatant of the solution was removed. Next, the residue was washed and dried at room temperature, and the magnetic biochar was obtained [20]. Different from the pyrolysis, the hydrothermal carbonization system is reacted at lower temperature with many kinds of biomass in a metal particle solution. These reactions are relatively milder reaction situations than the abovementioned methods [21].

2.2 Biochar properties for remediation of contamination soil

Biochar displays a tough morphological surface with honeycomb under the microscope. The inherent micropores engender biochar a comparatively excessive intrapore volume and low envelope density. Biochar consists frequently of amorphous, aromatic

carbon and possesses over abundant oxygen containing surface functional groups (C=O, -COOH, and -OH) and a disorderly stacked graphene sheet shape. Biochar largely has negatively charged surfaces that will increase the surface assimilation capability of cation species [22]. Thus, it plays a crucial position in improving nutrient retention in soil. The biochar capabilities and applications largely depend on their structural and physicochemical properties. So, it is vital to represent the structural and physicochemical properties of biochar before its use. Different feedstocks and pyrolysis method situations contribute to different structural and physical traits of biochar, including structural complexity, extent, porosity, particle size distribution, density, and mechanical strength [23]. During pyrolysis, biomass feedstock undergoes a variety of physical, chemical, and molecular changes. Pyrolysis circumstance and feedstock type considerably affect the structural and physicochemical traits of the ensuing biochar product. Such as the aromaticity of biochar usually increases, whereas the surface practicality decreases due to the fact that pyrolysis temperature is elevated. It is often an outcome of the innovative losses of aliphatic C-H, olefinic C=C, carbonyl, carboxyl, and hydroxyl groups at a higher temperature [24].

Biochar has been explored for mitigating soil heavy metal contamination. Many reported analysis indicates that biochar is capable of efficaciously immobilizing heavy metallic elements in soil and sorbing heavy metallic cations from water. Thus, biochar serves as a promising amendment for decreasing the eco-toxicity of heavy metal contaminated soils [24]). Biochar's high sorption capability together with high surface area applicable to immobilize contaminants. It is assumed that the contaminants will not be freed into the matrix until the biochar is degraded [25]. Biochar can also immobilize heavy metals through reduction. The oxygen functional group on the surface of biochar reduces the hexavalent chromium (Cr (VI)) to the trivalent (Cr (III)) via influencing its redox response. Cr (III) is usually nontoxic and tightly attached to soil particles, whereas Cr (VI) is very poisonous and mobiles [26].

3. Heavy metals contaminated soil

3.1 Sources of heavy metal contamination to soil and heavy metal toxic effects

The metals with relatively higher specific density compared to water ($>5 \text{ g/cm}^3$) are considered as heavy metals [27]. Naturally, heavy metals are found over the earth's crust in trace amount, so also considered as trace metals [28]. In past decades, the amounts of heavy metals are found to be increasing dramatically besides their natural occurrence. In the meantime, public health concerns due to the toxicity of these metals increased worldwide. Heavy metals such as lead (Pb), mercury (Hg), arsenic (As), lithium (Li), titanium (Ti), antimony (Sb), cadmium (Cd), chromium (Cr) are the most toxic metals with highly detrimental effects on human and animal organs and plant system [29]. Exposure to these metals beyond their permissible limit has life-threatening effects on biological world. Hg, Pb, As, Cd, and Cr are classified as top-priority toxic metal pollutants of significant concern.

Normally, the soil parent material itself contains most of the heavy metals in trace amount, which is not bioavailable. Rather anthropogenically added heavy metals have high bioavailability. There are different identified sources adding heavy metal contamination to soil, including agricultural practices, industrial and domestic effluents, natural and atmospheric sources. Sufficient Cd, Zn, Cr, and Ni will be generated due to wastewater, industrial wastes, and deposited sludge released from industrial

applications such as milling, electroplating, etching, tanning, textile and dye, metal casting and smelting, wood preservation and processing, photography, pharmaceutical printed circuit board (PCB), glass processing, manufacturing, etc. [30].

Most of the mismanaged anthropogenic activities are responsible for rapid contamination of soil with various toxic metals. Phosphate and nitrate fertilizers also contain variable amount of Cr, Cd, Ni, Pb, Hg, and Zn in which Cd is of main concern due to its accumulation in plant leaves. Pesticides, fungicides extensively used in agriculture, horticulture, and animal husbandries are the mixture of different compounds containing metals such as Cu, Hg, Fe, Pb, Zn. All these practices contribute to elevate the background concentration of heavy metals in soil. The agriculture practices, such as cattle manure, pig manure, and livestock manure, can add a large amount of Cu, Mn, Cd, Cr, Pb, and Zn to the soil. These ascribed to the compounds of livestock were containing various metals as the animal feed in the pig and poultry industry. And the feces containing metals of these animals were reused for land application. In the long run, these heavy metals will cause a large accumulation in the soil [31].

3.2 Heavy metal removal mechanism of biochar in soil

The heavy metal contamination soils and its management are a challenging issue. Because it is hard to mineralize them into other forms and their persistence. The remediation mechanism of biochar is different for different heavy metal pollutants. And for the same heavy metal ion, the adsorption mechanism is different when the biochar is different [32]. The removal mechanism of biochar acting on the bioavailable fraction of soil heavy metals is as follows: complexation, physical sorption, electrostatic attraction, ion exchange precipitation, etc. That can be able to reduce also their leachability [33]. Biochar rich in oxygen containing acidic functional groups (phenolic, carbonyl, lactonic, carboxylic, phenolic, and hydroxyl) plays significantly important role in binding (complexation) of heavy metals and metalloids onto the biochar surface as well as inner pores. Physical adsorption involves the removal of heavy metals by diffusion of metal ions into the pores of sorbent. Since biochar is the carbon material with a well-distributed pore networks including micropores (<2 nm), mesopores (2–50 nm), and macropores (>50 nm) [34]. Biochar surface is negatively charged. Heavy metal immobilization via electrostatic attractions takes place between metal ions and biochar's surface charge. This is the electrostatic attraction. Ion exchange from soil matrix to the surface of biochar is another method of metal fixation by biochar. The size of functional groups and metal species on the surface of biochar are the most important factors affecting the residual efficiency of heavy metals in the ion exchange process [35]. Precipitation is considered as the most common accountable mechanism for heavy metal immobilization by biochar. During the sorption process formation of solid(s), either in solution or on a surface is known as precipitation.

4. Experimental case study: Materials and methods

4.1 Field aging of biochar and separation of aged biochar particles

The work of the field aging of biochar was carried out in Wuhan City, Hubei Province (30°28'N, 114°25'E). The biochar used in this work was got from Zhengzhou

Lishe Environmental Protection Co., Ltd. in China. The biochar was made from the 3–5 mm corn straw pyrolysis at 500°C. Using the abovementioned biochar as raw material, the biochar field aging test was started in 2015. The biochar was added to the soil at a ratio of 1% (w/w) as biochar treatment, and the soil without biochar addition was as control (CK). Seven years later, we got the field-aged biochar by manually separating the biochar particles with a diameter greater than 3 mm from the soil by tweezers. We planted vegetables in the soil with or without biochar as usual during the past 7 years. The field-aged biochar is carefully washed with deionized water to remove soil particles attached to its surface and then dried at 35° C for 8 hours to eliminate moisture. The field-aged biochar (ABC) was obtained. Comparatively, the biochar purchased from Lishe Environmental Protection Company is relatively named fresh biochar (FBC). The appearance of soil, FBC, and ABC is shown in **Figure 1**.

4.2 Biochar characterization

4.2.1 pH and EC of biochar

We examined the EC and pH values of the biochar samples by deionized water at the ratio of 1: 5 (W/V). Conductivity meter (DDS-307A, Rex, China) and PH meter (pHs-3c, Rex, China) were equipped respectively.

4.2.2 Pore diameter and specific surface area (SSA) of biochar

A scanning electron microscopy (SEM, Tianmei, SU8010, China) was used for observing the surface morphology of biochar. Before imaging, biochar samples were sprayed with gold for 2 minutes to improve conductivity and imaging quality of the biochar. The pore diameter and the SSA were analyzed by a pore size analyzer and an automated surface area (Mike ASAP2020, USA). About 0.5 g of each biochar sample was degassed at 125° C for 3 hours, and then SSA was determined using Brunauer–Emmett–Teller (BET) equation according to N₂ adsorption/desorption data.

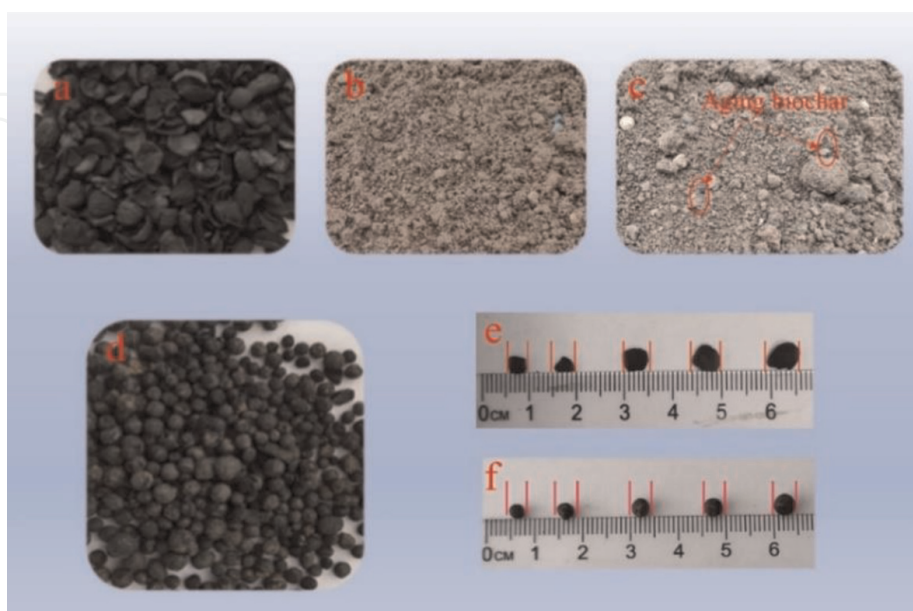


Figure 1. Appearances of FBC (a), ABC (d), original soil (b), the aged biochar-soil mixture with soil (c), and the particle size of FBC (e) and ABC (f). **Note:** FBC: Fresh biochar; ABC: Field-aged biochar.

4.2.3 The crystal structures and functional groups of biochar

X-ray powder diffractometer (XRD, Brooke, D8 ADVANCE) equipped with Cu K α radiation ($\lambda = 1.5406 \text{ \AA}$) was used for determining the crystal structures of biochar samples. The XRD pattern was acquired at 0.02° step size, $5^\circ/\text{min}$ scanning speed, and in the 2θ range of $5 \sim 90^\circ$. Fourier transform infrared spectroscopy (FTIR) (Thermo Fisher, Nicolet in10) and KBr were used for characterizing the functional groups on the surface of biochar. The spectral regions from 4000 to 400 cm^{-1} were recorded at a resolution of 2 cm^{-1} .

4.2.4 The elements contents of C, N, O, H, and S of biochar

The Elemental Analyzer (EA, Vario el cube) was used for analyzing the contents of C, N, O, H, and S elements in FBC and ABC samples with argon as a carrier gas. X-ray photoelectron spectroscopy (XPS, thermo escalab250xl, USA) was used to study the combined states of major elements in biochar. The elemental binding energy was corrected to C1s (284.8 eV) obtained in the experiment.

4.3 Batch adsorption experiment

4.3.1 Adsorption kinetics

In this experiment, 20 mg/L Cd^{2+} and Pb^{2+} solutions were used for subsequent adsorption experiments. Using 0.01 mol/l NaNO_3 solution as background electrolyte, dissolve CdCl_2 and PbCl_2 respectively to prepare 1 g/L Cd^{2+} and Pb^{2+} stock solutions, respectively. Then we adjust the initial pH of the stock solution to 5.0 ± 0.2 with 0.1 mol/L NaOH or HCl solution. The adsorption kinetics experiment was carried out at room temperature. About 0.15 g of ABC or FBC respectively was added to 150 ml of 20 mg/L Cd^{2+} and Pb^{2+} solution, shaken well at 180 RPM/min . The collection time intervals of all samples were $0.083, 0.25, 0.5, 1, 2, 4, 6, 8, 12,$ and 24 h , respectively. There were three replicates per treatment. All samples were filtered through a $0.45 \mu\text{m}$ membrane in the adsorption experiments. Inductively coupled plasma atomic emission spectrometry (ICP-AES) (Icpe-9000, Shimadzu Corporation, Japan) was used to determine the concentrations of Pb^{2+} and Cd^{2+} and the changes of substituted $\text{Na}^+, \text{Ca}^{2+}, \text{K}^+,$ and Mg^{2+} .

The adsorption capacities of biochar for Cd^{2+} and Pb^{2+} were calculated according to the formula (1):

$$Q_e = \frac{(C_0 - C_e)V}{m} \quad (1)$$

C_e (mg/L): the remaining concentration of Pb^{2+} and Cd^{2+} in the solution; C_0 (mg/L): the initial concentration of Pb^{2+} and Cd^{2+} in the solution; V (mL): the volume of heavy metal solution; m (g): the dosage of biochar.

Two different models were used to fit the adsorption kinetic data. The formula is as follows:

$$Q_t = Q_e(1 - e^{-k_1t}) \quad (2)$$

$$Q_t = \frac{Q_e^2 k_2 t}{1 + Q_e k_2 t} \quad (3)$$

Q_t : the adsorption capacity of Cd^{2+} or Pb^{2+} on biochar at time t ; Q_e (mg/g): the adsorption capacity of Cd^{2+} or Pb^{2+} on biochar at time equilibrium; t (h) is the adsorption time; k_1 (h^{-1}): the rate constant of the pseudo-first-order kinetic equation; k_2 (g/mg/h) the rate constant of pseudo-second-order kinetic equation.

4.3.2 Biochar isotherms adsorption

The adsorption isotherms were conducted as follows: add 0.02 g of biochar to 20 ml of Cd^{2+} and Pb^{2+} Solution for adsorption isotherm, and the initial concentration is 5–120 mg/L. Equilibrium adsorption was performed at room temperature for 24 h. The rest of the operation is the same as the adsorption kinetics.

The adsorption isotherms was disclosed using Langmuir and Freundlich models. The equations are listed as follows:

$$Q_e = \frac{Q_m b C_e}{1 + b C_e} \quad (4)$$

$$R_L = 1/(1 + b C_0) \quad (5)$$

$$Q_e = K_f C_e^{1/n} \quad (6)$$

Q_e (mg/g): the amounts of Cd^{2+} or Pb^{2+} adsorbed on biochar; Q_m (mg/g): the maximum saturated adsorption capacity of biochar; C_0 (mg/L): the initial concentration of Cd^{2+} or Pb^{2+} ; C_e (mg/L): the equilibrium concentration of Cd^{2+} or Pb^{2+} ; b (L/mg) and K_f ((mg/g) (mg/L)⁻ⁿ): the corresponding constants of Langmuir and Freundlich; n : the Freundlich constant related to the surface site heterogeneity; R_L : the dimensionless constant separation factor.

4.3.3 Biochar saturated adsorption

Biochar saturation adsorption experiments were executed on the basis of adsorption kinetics. About 0.5 g biochar and 100 mL 100 mg/L Cd^{2+} or Pb^{2+} solution were mixed and shaken for 24 h at 180 rpm/min at 25°C. The mixture liquid was filtered by 0.45 μ m acetate membrane. ICP-AES was used for determining the concentrations of Cd^{2+} and Pb^{2+} in the mixed solution before and after adsorption by biochar.

4.3.4 Toxicity characteristic leaching procedure (TCLP)

The TCLP test was with the solution. The extraction solution was obtained by dissolving glacial acetic acid with 5.7 mL into the deionized water to a total volume of 100 mL. And the solution's initial pH was adjusted at 2.9 ± 0.05 . Next, the 0.25 g of biochar was added into the extraction solution with 10 ml and shaken the solution at 180 rpm/min for 18 h at 25 °C. Then, the Cd^{2+} and Pb^{2+} contents in the extraction solution were analyzed using ICP-AES after being filtered through a 0.45 μ m acetate membrane.

$$TCLP_{-Cd/Pb} = \frac{q_1}{q_2} \times 100\% \quad (7)$$

q_1 (mg/g): the contents of Cd^{2+} and Pb^{2+} in the extraction solution of TCLP; q_2 (mg/g): the biochar's total saturated sorption of Cd^{2+} and Pb^{2+} .

4.3.5 Statistical analysis

The statistical analysis in the paper is using the SPSS23.0 software (SPSS Inc., USA). Data are presented as mean \pm standard deviation. One-way analysis of variance (ANOVA) with a least significant difference (LSD) at a 0.05 significance level was used for the standard analysis. XPS and XRD data were analyzed with Advantage and Jade6.5 software, respectively. Origin Pro 2018 (OriginLab, USA) and Microsoft Excel 2016 (Microsoft Corporation, USA) were used for drawing the figures and tables.

5. Experimental case study: results and discussion

5.1 The capabilities of field-aged biochar

5.1.1 The microstructure of field-aged biochar

Compared with FBC, the surface of ABC became smoother after 7 years of application in the soil as shown in **Figure 2(c)** and **(d)**. And there were no small particles attached on its surface. However, the surface of FBC was rough and has some attached aggregates shown in **Figure 2(a)** and **(b)**. These SEM results illustrated that the small particles attached on FBC surface may be labile fractions or soluble substances (e.g., CaCO_3 as shown in **Figure 3**) from the pyrolysis processes of corn straw [36].

5.1.2 The surface morphology of field-aged biochar

The SSA data demonstrated that, compared with the FBC, the ABC's pore volume, the SSA, and size were 0.02 ml/g, 8.32 m^2/g , and 9.62 nm. While the FBCs were 0.0017 ml/g, 2.98 m^2/g , and 2.32 nm, respectively (**Table 1**). These demonstrated that the SSA, pore volume, and pore size of ABC increased by 179%, 1076%, and 314% compared with FBC.

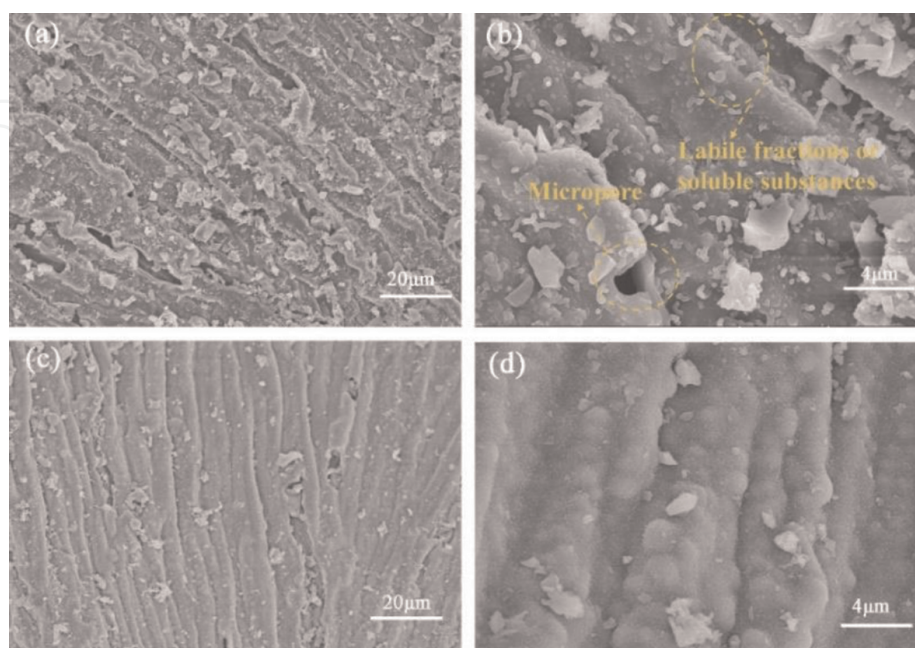


Figure 2. Scanning electron micrographs of FBC (a, b) and ABC (c, d).

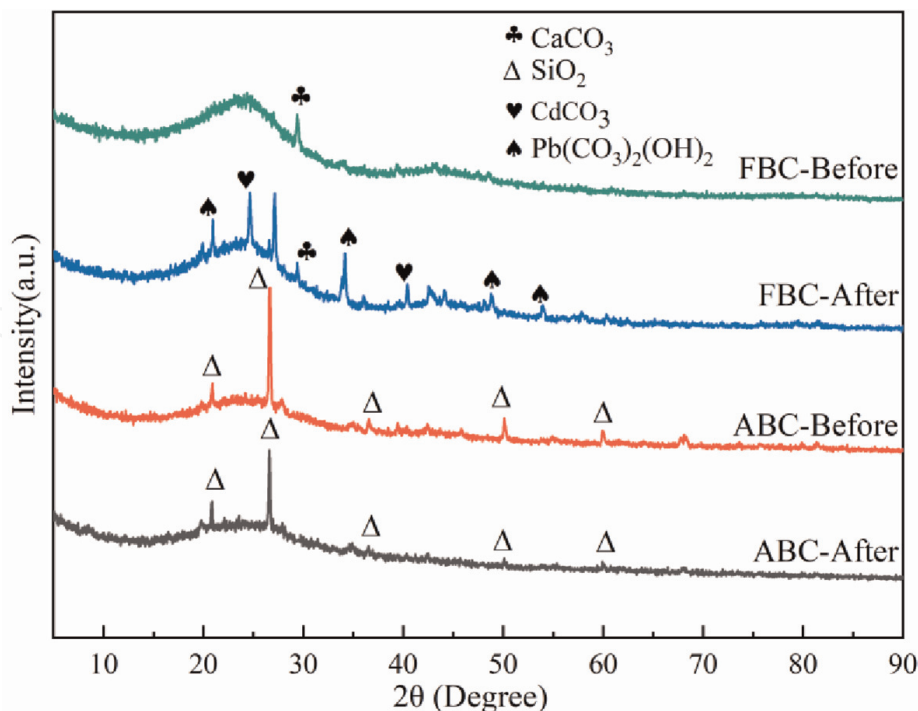


Figure 3. XRD patterns of FBC and ABC before and after adsorption of heavy metals.

5.2 The chemical properties of field-aged biochar

5.2.1 Potential of hydrogen (pH) of field-aged biochar

The properties of biochar are presented in **Table 1**. The pH of ABC was 5.83 as acidic while FBC was 8.87 displayed alkaline. This demonstrated that biochar in field aging process remarkably decreased the pH.

5.2.2 The elemental analysis of field-aged biochar

Table 2 shows the elemental contents of ABC and FBC. The C content in ABC was 46.89%, decreased considerably compared with the content in FBC, which is 81.01. The C content in ABC was 21.26% while was 12.47% in FBC. The atomic ratios, including H:C O:C and (N+O+S):C, increased notably with aging, suggesting that ABC was highly oxidized and exhibited lower aromaticity than FBC.

5.2.3 The crystal structures of field-aged biochar

Figure 3 shows the crystal structures of FBC and ABC before and after the reaction with heavy metal, which were investigated by XRD and analyzed using Jade6.5 PDF cards. In ABC, there is a strong peak appearing at 26.6° where was assigned to the characteristic diffraction peak of SiO_2 either before or after the absorption of heavy metal [37]. However, there is a peak located at 29.5° where is the crystalline structures of CaCO_3 in FBC in the XRD pattern before the absorption of heavy metal. And interestingly, the diffraction peaks appearing at $2\theta = 30.33^\circ$, 20.97° , and 24.79° after the heavy metal ions are adsorbed by FBC can be ascribed to CdCO_3 , $\text{Pb}(\text{CO}_3)_2(\text{OH})_2$, and PbCO_3 [20]. Totally, the intensity of the characteristic peaks of CaCO_3 and SiO_2 in FBC and ABC was obviously weakened or disappeared after the absorption with heavy

Sample	FBC	ABC
C (%)	81.01	46.89
H (%)	2.77	3.02
O (%)	12.47	21.26
N (%)	0.40	6.61
S (%)	0.00	1.85
H:C	0.03	0.06
O:C	0.15	0.45
(N + O + S):C	0.16	0.63
SSA (m ² /g)	2.98	8.32
Total pore volume (cm ³ /g)	0.0017	0.02
Average pore diameter (nm)	2.32	9.62
pH	8.87 ± 0.01	5.83 ± 0.02
EC (μS/cm)	142.20 ± 0.00	252.00 ± 0.01

Values are mean ± SD (n = 3).

Table 1.
The physicochemical properties of FBC and ABC.

Binding energy (eV)	Area of samples (%)				Attribution
	FBC	FBC-Cd,Pb	ABC	ABC-Cd,Pb	
284.8 ± 0.1	57.33	58.2	42.92	51.6	C-C/ C=C
285.4 ± 0.1	19.38	16.94	27.34	24.69	C-O-C/C-OH
286.4 ± 0.3	18.24	18.17	22.61	18.43	C=O
289.1 ± 0.2	5.05	6.7	7.13	5.28	O-C=O/Carbonate

Table 2.
The data of XPS analysis of C1s for samples.

metal. We can conclude that precipitation may be one of the main mechanisms for Cd²⁺ and Pb²⁺ removal by FBC.

5.2.4 The functional groups of field-aged biochar

Figure 4 shows the FTIR spectra of ABC and FBC before and after the adsorption. There were some differences in the types and intensity of surface functional groups on ABC and FBC. The main functional groups on ABC were including C=O [38], COO⁻ [39], Si-O-Al, C-H, Al-O-Si [41], Si-O-Si [37]. While the functional groups on FBC were C=C, COOH/CHO, phenolic -OH bending, CO₂-3, C-O, and C-C, the aromatic ring C-H, the aromatic C-H [41]. The -OH and C-H were in all samples. There were also changes of FBC/ABC between before and after the adsorption of heavy metals. After FBC adsorbs metal ions, the peak waves of C = C, C = O and aromatic hydrocarbons were shifted. This may be the result of chelation of heavy metal ions with

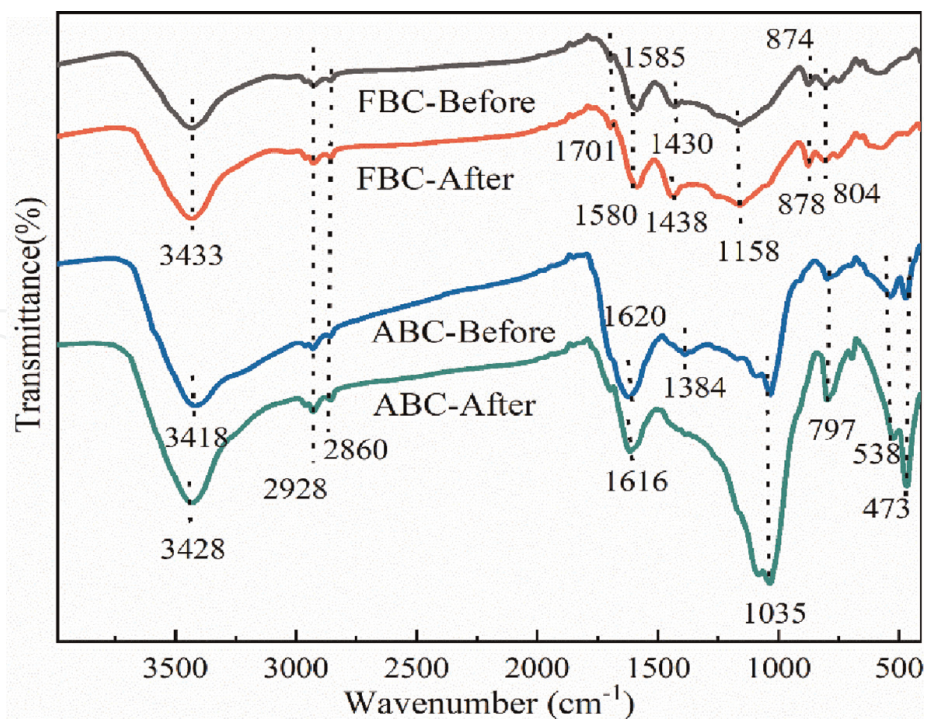


Figure 4. FTIR spectroscopy of FBC and ABC before and after adsorption. Note: Peak at 3418–3433 cm^{-1} : -OH; peak at 2950 cm^{-1} and 2860 cm^{-1} : Saturated C-H; peak at 1620 cm^{-1} : C=O; peak at 1585 cm^{-1} : Aromatic C=C; peak at 1430 cm^{-1} : -COOH/CHO; phenolic -OH bending; CO₂-3; peak at 1384 cm^{-1} : COO⁻; peak at 1158 cm^{-1} : C-O and C-C; peak at 1158 cm^{-1} : Si-O-Si or Si-O-Al asymmetric; peak at 874 cm^{-1} : Aromatic ring C-H bonds; peak at 804 cm^{-1} : Aromatic C-H; peak at 797 cm^{-1} : Aromatic C-H stretching; peak at 538 cm^{-1} : The symmetric of Al-O-Si; peak at 538 cm^{-1} : The antisymmetric of Si-O-Si.

aromatic structure of biochar (cation- π interaction). In addition, we also found that the atomic ratio of (N+O+S): C and H: C in ABC increased significantly, which can measure the polarity and aromaticity of biochar. These indicated that the aromaticity of ABC decreased while the polarity increased. This would reduce the stability of heavy metal ions, which passivated by biochar and the heavy metal would be released to the soil inducing secondary pollution. These results were consistent with the increments of TCLP leaching rate of Cd²⁺ and Pb²⁺ in ABC.

5.2.5 The combination state of main elements in field aging biochar

Figure 5 shows that the C, O, N, S, Si, and Al were observed in ABC (**Figure 5(c)**), while only C and O elements were in FBC (**Figure 5(a)**) before the heavy metal absorption. And O element is more in ABC than in FBC interestingly. That the O:C in ABC was 0.45 while was 0.15 in FBC. This ascribed to the O-containing functional groups of biochar markedly increased after aging in field. Data as showed in **Table 2**, the C1s spectrum were divided into four peaks: 285.4 \pm 0.1 eV (C-O), 284.8 \pm 0.1 eV (C-C/C=C), 289.1 \pm 0.2 eV (O-C=O or carbonate), and 286.4 \pm 0.3 eV (C=O). The relative proportion of C-C/C=C, C-O, C=O, and O-C=O/carbonate in ABC were 42.92%, 27.34%, 22.61%, and 7.13% respectively, while they were 57.33%, 19.38%, 18.24%, and 5.05% in FBC. That is, the ABC's relative contents of C-O, C=O, and O-C=O functional groups were dramatically higher than that of FBC. During the field aging process, due to the oxidation or weathering of persistent free radicals in the soil, oxygen-containing functional groups, including phenolic groups and carboxyl, were

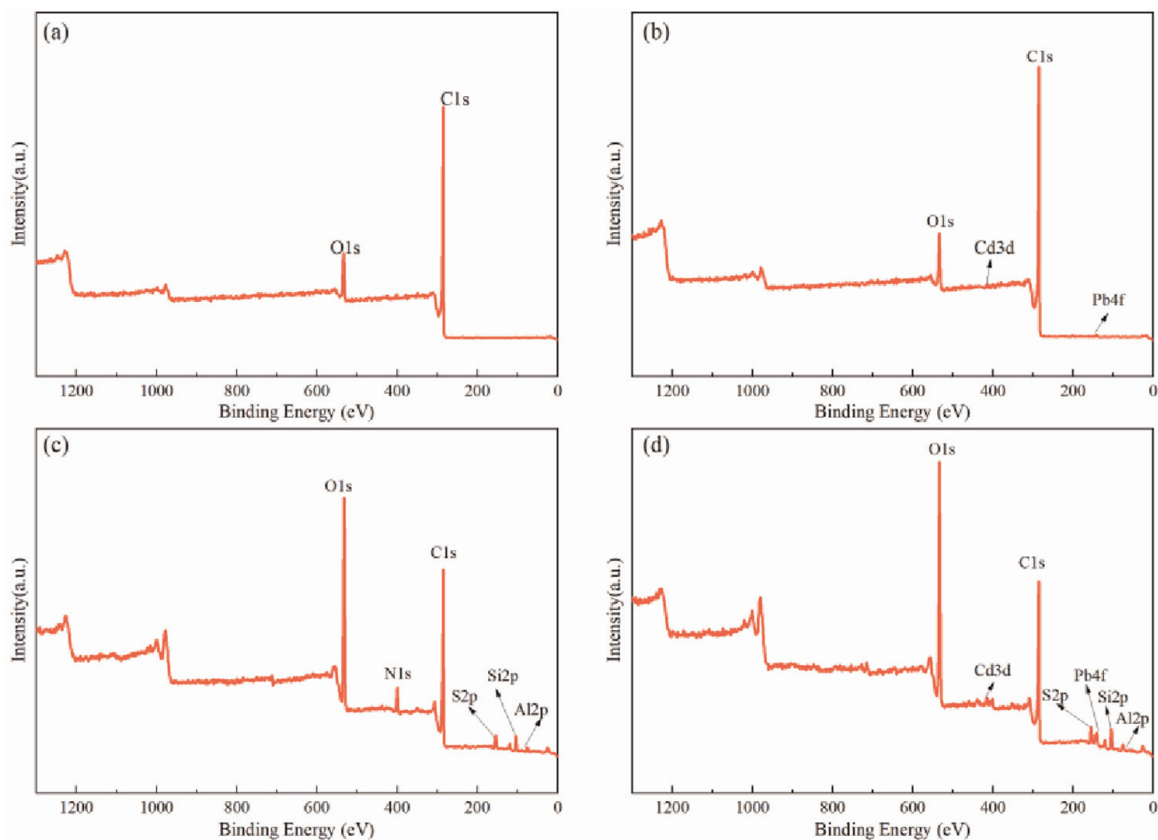


Figure 5.
XPS spectra for typical survey scan of FBC (a, b) and ABC (c, d) before and after adsorption.

formed on the surface of biochar [42]. This will contribute to an increase in the relative contents of C=O, O—C=O, and C—O. **Figure 6** shows that the peaks of Cd3d and Pb4f were observed in FBC and ABC before and after the adsorption of heavy metal. It was concluded that Cd²⁺ and Pb²⁺ were successfully adsorbed on the surface of biochar. It has been proved that the peaks of 412.5 eV and 405.6 eV belong to Cd 3d^{3/2} and Cd 3d^{5/2}, respectively. This indicated that Cd exists in the form of Cd—O through complexation with hydroxyl (—OH) or diprotic oxygen (—O—) on the surface of biochar [43, 44]. The peaks of Pb4f appeared at around 144.4 eV and 139.4 eV, which can be attributed to Pb—O—C and Pb—O [45].

5.2.6 The discussion of chemical properties of biochar

The pH of biochar was reduced by three units after being aged in the agricultural field for 7 years. This change can be attributed to the alkaline substances in FBC leached out [5]. During aging, the alkaline substances were dissolving. In addition, the decrease in basicity of biochar may be due to O-containing functional groups' formation on the biochar's surface. These can be well explained by elemental analysis and XPS. The analysis of elements showed that the O:C of FBC is 0.15 while the O:C of ABC was increased to 0.45. That is a representative of the oxidation level of biochar. XPS results indicated that the relative content of C=O, C—O, and O—C=O functional groups of FBC were dramatically lower than that of ABC. During the field aging process, due to the oxidation by persistent free radicals in soil or weathering effects, including phenolic groups and carboxyl, oxygen-containing functional groups were

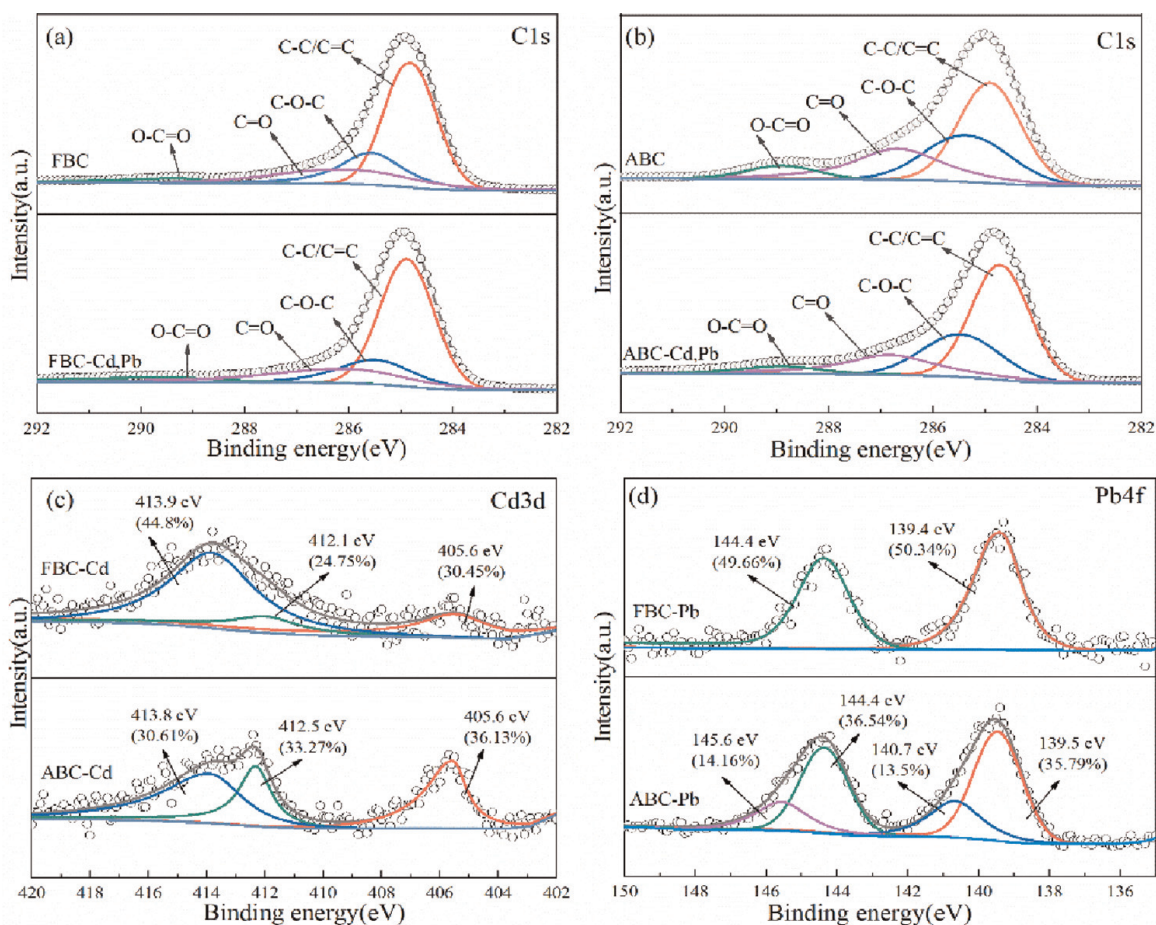


Figure 6. XPS spectra of C1s, Cd3d, and Pb4f for FBC and ABC before and after adsorption.

formed on the surface of biochar. These lead to the increase of the relative content of O=C=O, C=O, and C-O. However, the formation of acidic functional groups on the surface of biochar, such as carboxyl and phenol groups, can cause the biochar's lower pH value [12].

It was further confirmed that more O-containing functional groups were formed on aged biochar surface during aging in field [5]. Biochar has large SSA and abundant pore structure. In our study, the average pore size and SSA of ABC increased by 4331.39% and 279.19% compared with FBC, respectively. Even more interesting is that the total pore volume in ABC increased more than 9.9-fold compared with FBC. The freeze-thaw cycles and rainfall events of biochar in soil maybe related with these changes. The expansion and elimination of water molecules also occur in biochar during freeze-thaw cycles [12]. As a result, the SSA of the biochar increases. As well, aging in field may also influence the functional groups and elemental composition of biochar surface. In this study, the relative contents of S, O, and N in ABC increased significantly compared with FBC. While the relative content of C decreased in ABC compared with FBC. These results were in accordance with the results of the pre-venients [8]. It was found that the O content of biochar's surface increased while the C content decreased after 5 years in the field soil, and the o content increased. These indicated the dissolution of unstable C during the aging process of biochar [12, 46]. Furthermore, the results of XPS indicate that the amounts of Al and Si in ABC increased, implying that soil minerals could have been attached on biochar surface during field aging. This result was also reported in previous studies.

5.3 Biochar sorption experiments

5.3.1 The kinetic adsorption of field-aged biochar

Figure 7 shows the adsorption kinetics of Cd^{2+} and Pb^{2+} on FBC and ABC in the single-metal (Figure 7(a and b)) and binary-metal (Figure 7(c, d)) systems. Correspondingly, Table 3 gives the parameters fitted by pseudo first-order model and

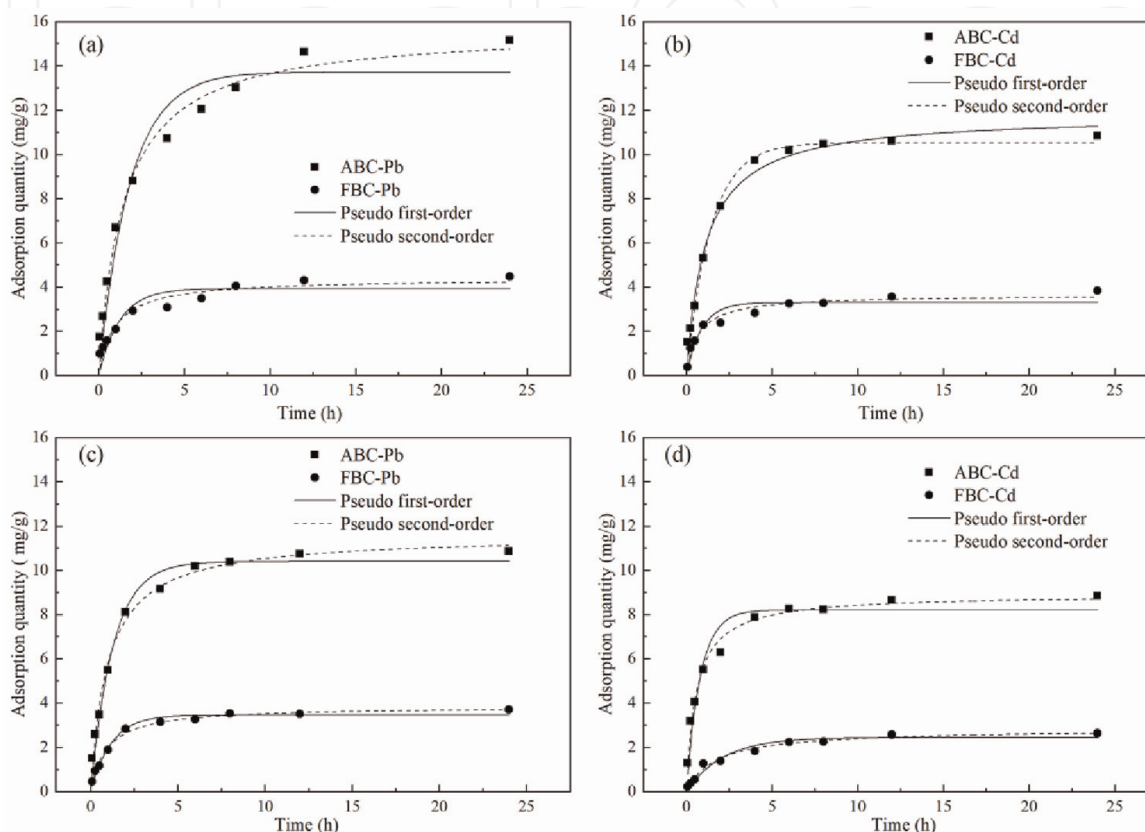


Figure 7. Kinetic adsorption of Cd^{2+} and Pb^{2+} by PBC and ABC in single- (a, b) and binary-metal (c, d) systems.

Adsorption	Biochars	Pseudo first-order			Pseudo second-order		
		R^2	k_1 (h)	Q_e (mg/g)	R^2	k_2 (g/h/mg)	Q_e (mg/g)
Single	FBC-Pb	0.8623	0.8183	3.92319	0.9754	0.2432	4.3774
	ABC-Pb	0.95141	0.5487	13.70752	0.98771	0.0435	15.6564
	FBC-Cd	0.9160	1.1416	3.2934	0.96737	0.40082	3.6364
	ABC-Cd	0.98975	0.07578	11.78350	0.99512	0.69917	10.52060
Binary	FBC-Pb	0.9794	0.8554	3.45187	0.9901	0.2871	3.8336
	ABC-Pb	0.9809	0.7792	10.3918	0.9917	0.0870	11.5773
	FBC-Cd	0.96701	0.47213	2.45183	0.98320	0.20870	2.81340
	ABC-Cd	0.94195	1.22718	8.20247	0.98758	0.19306	8.90370

Table 3. Fitting parameters of pseudo-first-order and pseudo-second-order kinetics Cd^{2+} and Pb^{2+} by FBC and ABC single- and binary-metal systems.

pseudo first-order model. From the perspective of R^2 in **Table 3**, the pseudo second-order kinetic model ($R^2 = 0.9674\text{--}0.9917$) was better fit for the Cd^{2+} and Pb^{2+} adsorption kinetics data for FBC and ABC in the single-metal and binary-metal systems, compared with the pseudo first-order model ($R^2 = 0.8623\text{--}0.9898$). In addition, the calculated Q_e values based on the pseudo second-order model were approximately the experimental Q_e values. Overall, the adsorption of two metal ions on ABC or FBC increased dramatically within 2.5–3.0 hours and then approached to a flat with the augment of reaction time shown in **Figure 7(a–d)**. And the adsorption quantity on Cd^{2+} and Pb^{2+} of ABC was stronger than FBC either in the single-metal or binary-metal system. It was interesting that the capacity of equilibrium adsorption in single-metal system was higher than that of the binary-metal system. While the capacity of its total adsorption was weaker. That is, ABC and FBC reach the adsorption equilibrium at 8 h in the binary-metal system, while at 12 h in the bimetallic system. These were indicating that there was a competitive relationship between Cd^{2+} and Pb^{2+} .

5.3.2 The isothermal adsorption of field-aged biochar

Figure 8 shows the isothermal adsorption of Cd^{2+} and Pb^{2+} on FBC and ABC in the single- (**Figure 8(a, b)**) and binary-metal (**Figure 8(c, d)**) systems. Correspondingly, **Table 4** gives the fitting parameters of the Langmuir and Freundlich isothermals for Cd^{2+} and Pb^{2+} by FBC and ABC in single- and binary-metal systems. As shown in **Figure 8**, Langmuir model due to its higher correlation coefficient ($R^2 = 0.96013\text{--}0.9910$) was more reasonable than Freundlich model ($R^2 = 0.7924\text{--}0.9679$) in this isothermal adsorption experimental data analyses. **Figure 8** shows that at low initial concentrations, the adsorption capacity of eight ABCs or FBCs increased with the

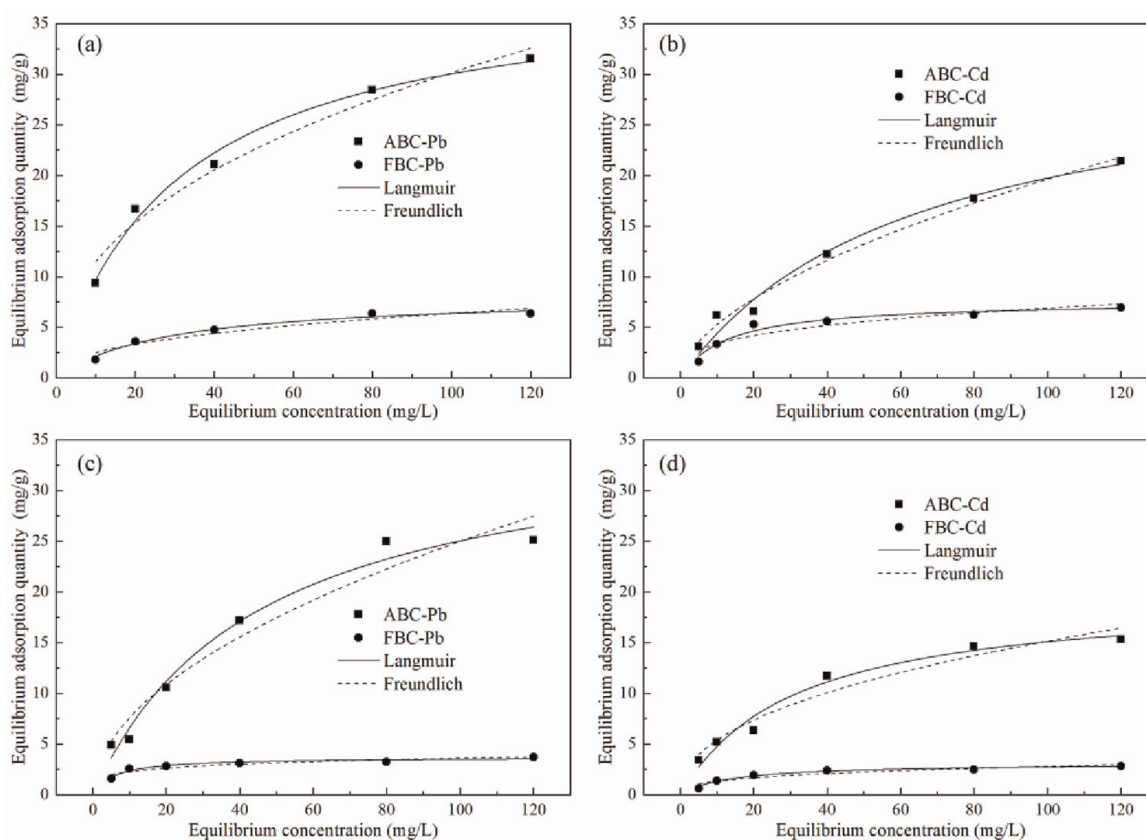


Figure 8. Isothermal adsorption of Cd^{2+} and Pb^{2+} by FBC and ABC in single- (a, b) and binary-metal (c, d) systems.

Adsorption	Biochars	Langmuir parameters			Freundlich parameters		
		R ²	b	Q _m	R ²	K _f	1/n
Single	FBC-Pb	0.9796	0.03572	8.1343	0.91864	1.0021	0.40162
	ABC-Pb	0.9914	0.03267	39.2158	0.97437	4.3564	0.42020
	FBC-Cd	0.96033	0.07847	7.57289	0.86456	1.6577	0.30922
	ABC-Cd	0.98236	0.01584	32.1566	0.98122	1.4110	0.57164
Binary	FBC-Pb	0.94327	0.17694	3.68653	0.87602	1.47112	0.19475
	ABC-Pb	0.98103	0.00298	36.2279	0.95295	2.30530	0.51751
	FBC-Cd	0.97325	0.07456	3.09823	0.87805	0.65300	0.31578
	ABC-Cd	0.97655	0.03210	19.74660	0.95364	1.933256	0.44694

Table 4. Fitting parameters of Langmuir and Freundlich isotherms for Cd²⁺ and Pb²⁺ by FBC and ABC in single- and binary-metal systems.

increasing of initial concentration of Cd²⁺ and Pb²⁺ and then gradually slowed down when the biochar reached saturation. It has been known that in Langmuir isotherm the separation factor R_L commonly used to evaluate the affinity between the adsorbent and the adsorbed material [40]. They are as follows: when R_L > 1, adsorption is unfavorable; when R_L = 1, adsorption is linear; when 0 < R_L < 1, adsorption is favorable; when R_L = 0, adsorption is nonlinear; and when R_L < 0, adsorption is irreversible [14, 47]. In this experiment, the initial concentrations of Cd²⁺ and Pb²⁺ were ranged from 5 to 120 mg/L (Table 4). The R_L values of FBC-Pb, FBC-Cd, ABC-Pb, and ABC-Cd were between 0 and 1. These results indicated that both ABC and FBC were favorable for Cd²⁺ and Pb²⁺ adsorption. In addition, Table 4 shows that all 1/n values were in the range of 0–1 in this study, indicating that adsorption is also favorable [48]. The above analysis illustrated that the adsorption of Cd²⁺ and Pb²⁺ on FBC and ABC was monolayer adsorption.

5.3.3 The metal leachability and bioavailability of field-aged biochar

In order to understand the metal leachability and bioavailability of ABC, we take the leaching characteristics of Cd²⁺ and Pb²⁺ in FBC and ABC by TCLP method. The results showed that the concentration of Cd²⁺ and Pb²⁺ in TCLP leachate was 39.21% and 28.62% in ABC while was 24.08% and 21.24%, respectively in FBC. This implied that the adsorption mechanisms of ABC for Cd²⁺ and Pb²⁺ were different from FBC. At same time, the increase of TCLP leachability of Cd²⁺ and Pb²⁺ suggesting the stability of ABC to immobilized heavy metals was significantly reduced.

5.3.4 The discussion of biochar sorption

The results of isothermal and kinetic adsorption experiments showed that the pseudo-secondary kinetic and Langmuir model were more fitted with the adsorption of metal ions by FBC and ABC. FBC and ABC immobilize Cd²⁺ and Pb²⁺ in binary metal system as a chemical reaction as confirmed by the above results [20, 49, 50]. ABC adsorbs more heavy metal ions than FBC. These ascribed to the aged biochar having more oxygen-containing functional groups and a larger SSA. These indicated

that ABC surface has more chemisorption active sites. Additionally, the biochar can well serve as a habitat for microorganisms, such as bacteria and fungi, due to its abundant porous structure.

In addition, the active component carbon and mineral nutrients in biochar can be used as its energy source by microorganisms in the soil environment [8, 36]. Therefore, it is likely that microorganisms will attach to the ABC surface after it is applied to the soil. Furthermore, the adsorption of heavy metals may be promoted by the beneficial microorganisms immobilized on biochar. It has been reported that the combined application of biochar and bacteria can improve the adsorption of heavy metals [33]. There are some possible mechanisms for the interaction between bacteria, biochar, and heavy metal ions. First, the respiration of bacterial cells attached to the surface of biochar form metal carbonate precipitates. Second, new adsorption sites were formed by bacteria colonized of biochar [13]. Third, bacterial cells are as transport carriers between heavy metals and biochar. That is, the heavy metal ions in the soil solution are first transferred to the cells, and then the cells adsorbed on the biochar and actively pumped out of the bacterial cells [51].

6. Conclusions

In conclusion, under field conditions, the physicochemical properties of biochar have changed in soil after 7 years of field aging. The pore volume and SSA of biochar increased with field aging, owing to the dissolution of unstable carbon or carbides in biochar. FTIR and XPS results proved that there were abundant O-containing functional groups on the surface of aged biochar. The results of adsorption kinetics and adsorption isotherm showed that the adsorption of heavy metal ions on ABC and FBC surface was controlled by chemical adsorption. FBC immobilizes Cd^{2+} and Pb^{2+} mainly through cation exchange, co-precipitation, and cation- π interaction. Whereas the main mechanism of ABC removing Cd^{2+} and Pb^{2+} may be the cation exchange and surface complexation. Compared with that of FBC, the adsorption performance of ABC for Cd^{2+} and Pb^{2+} is improved due to the increases of O-containing functional groups and SSA in ABC. Nevertheless, the stability of ABC to immobilized heavy metals was significantly reduced.

Acknowledgements

This study was financially supported by the Projects of National Natural Science Foundation of China (31201618), China Agriculture Research System (CARS-23-G27).

IntechOpen

Author details


Run-Hua Zhang^{1*}, Lin-Fang Shi¹, Zhi-Guo Li², Guo-Lin Zhou¹, Yan-Lan Xie¹,
Xing-Xue Huang¹, An-Hua Ye¹ and Chu-Fa Lin¹

1 Wuhan Academy of Agricultural Sciences, Wuhan, China

2 Key Laboratory of Aquatic Botany and Watershed Ecology, Wuhan Botanical
Garden of Sciences, Wuhan, China

*Address all correspondence to: rhzhanag0508@126.com

IntechOpen

© 2022 The Author(s). Licensee IntechOpen. This chapter is distributed under the terms of the Creative Commons Attribution License (<http://creativecommons.org/licenses/by/3.0>), which permits unrestricted use, distribution, and reproduction in any medium, provided the original work is properly cited. 

References

- [1] Gong X, Huang D, Liu Y, Zou D, Hu X, Zhou L, et al. Nanoscale zerovalent iron, carbon nanotubes and biochar facilitated the phytoremediation of cadmium contaminated sediments by changing cadmium fractions, sediments properties and bacterial community structure. *Ecotoxicology and Environmental Safety*. 2021;**208**:111510. DOI: 10.1016/j.ecoenv.2020.111510
- [2] Li X, Xiao J, Salam MMA, Ma C, Chen G. Impacts of bamboo biochar on the phytoremediation potential of *Salix psammophila* grown in multi-metals contaminated soil. *International Journal of Phytoremediation*. 2021;**23**:387-399. DOI: 10.1080/15226514.2020.1816893
- [3] Raeisi S, Motaghian H, Hosseinpour AR. Effect of the soil biochar aging on the sorption and desorption of Pb²⁺ under competition of Zn²⁺ in a sandy calcareous soil. *Environmental Earth Sciences*. 2020;**79**(6):148. DOI: 10.1007/s12665-020-8891-y
- [4] Rathnayake D, Rego F, Van Poucke R, Bridgwater AV, Masek O, Meers E, et al. Chemical stabilization of Cd-contaminated soil using fresh and aged wheat straw biochar. *Environmental Science and Pollution Research International*. 2021;**28**:10155-10166. DOI: 10.1007/s11356-020-11574-6
- [5] Xu Z, Xu X, Tsang DCW, Cao X. Contrasting impacts of pre- and post-application aging of biochar on the immobilization of Cd in contaminated soils. *Environmental Pollution*. 2018;**242**:1362-1370. DOI: 10.1016/j.envpol.2018.08.012
- [6] Lam YY, Lau SSS, Wong JWC. Removal of Cd(II) from aqueous solutions using plant-derived biochar: Kinetics, isotherm and characterization. *Bioresource Technology Reports*. 2019;**8**:100323. DOI: 10.1016/j.biteb.2019.100323
- [7] Su Y, Wen Y, Yang W, Zhang X, Xia M, Zhou N, et al. The mechanism transformation of ramie biochar's cadmium adsorption by aging. *Bioresource Technology*. 2021;**2021**(330):124947. DOI: 10.1016/j.biortech.2021.124947
- [8] Dong X, Li G, Lin Q, Zhao X. Quantity and quality changes of biochar aged for 5 years in soil under field conditions. *Catena*. 2017;**159**:136-143. DOI: 10.1016/j.catena.2017.08.008
- [9] Nguyen, Wallace HM, Xu C-Y, Zwieten L(V), Hanweng Z, Xu Z, et al. The effects of short term, long term and reapplication of biochar on soil bacteria. *Science of the Total Environment*. 2018;**636**:142-151. DOI: 10.1016/j.scitotenv.2018.04.278
- [10] Wu Z, Zhang X, Dong Y, Xu X, Xiong Z. Microbial explanations for field-aged biochar mitigating greenhouse gas emissions during a rice-growing season. *Environmental Science and Pollution Research International*. 2018;**25**:31307-31317. DOI: 10.1007/s11356-018-3112-x
- [11] Zhang, Huang Q. Effect mechanism of biochar's zeta potential on farmland soil's cadmium immobilization. *Environmental Science and Pollution Research International*. 2019;**26**:19738-19748. DOI: 10.1007/s11356-019-05298-5
- [12] Wang L, O'connor D, Rinklebe J, Ok YS, Tsang DCW, Shen Z, et al. Biochar aging: Mechanisms, physicochemical changes, assessment, and implications for field applications. *Environmental Science & Technology*.

2020;**54**:14797-14814. DOI: 10.1021/acs.est.0c04033

[13] Tan L, Ma Z, Yang K, Cui Q, Wang K, Wang T, et al. Effect of three artificial aging techniques on physicochemical properties and Pb adsorption capacities of different biochars. *Science of the Total Environment*. 2020;**2020**(699):134223. DOI: 10.1016/j.scitotenv.2019.134223

[14] Lin Q, Zhang L, Riaz M, Zhang M, Xia H, Lv B, et al. Assessing the potential of biochar and aged biochar to alleviate aluminum toxicity in an acid soil for achieving cabbage productivity. *Ecotoxicology and Environmental Safety*. 2018;**161**:290-295. DOI: 10.1016/j.ecoenv.2018.06.010

[15] Mia S, Dijkstra FA, Singh B. Aging induced changes in Biochar's functionality and adsorption behavior for phosphate and ammonium. *Environmental Science & Technology*. 2017;**26**:1-26. DOI: 10.1021/acs.est.7b00647

[16] He E, Yang Y, Xu Z, Qiu H, Yang F, Peijnenburg W, et al. Two years of aging influences the distribution and lability of metal(loid)s in a contaminated soil amended with different biochars. *Science of the Total Environment*. 2019;**673**:245-253. DOI: 10.1016/j.scitotenv.2019.04.037

[17] Godwin PM, Pan Y, Xiao H, Afzal MT. Progress in preparation and application of modified biochar for improving heavy metal ion removal from wastewater. *Journal of Bioresources and Bioproducts*. 2019;**4**: 31-42. DOI: 10.21967/jbb.v4i1.180

[18] Murtaza G, Ahmed Z, Usman M. Feedstock type, pyrolysis temperature and acid modification effects on physiochemical attributes of biochar and soil quality. *Arabian Journal of*

Geosciences. 2022;**15**:305. DOI: 10.1007/s12517-022-09539-9

[19] Yang F, Zhang S, Sun Y, Du Q, Song J, Tsang D. A novel electrochemical modification combined with one-step pyrolysis for preparation of sustainable thorn-like iron-based biochar composites. *Bioresource Technology*. 2019;**274**:379-385. DOI: 10.1016/j.biortech.2018.10.042

[20] Zhou N, Zu J, Feng Q, Chen H, Li J, Zhong ME, et al. Effect of pyrolysis condition on the adsorption mechanism of heavy metals on tobacco stem biochar in competitive mode. *Environmental Science and Pollution Research International*. 2019;**26**:26947-26962. DOI: 10.1007/s11356-019-05917-1

[21] Yi Y, Huang Z, Lu B, Xian J, Fang Z. Magnetic biochar for environmental remediation: A review. *Bioresource Technology*. 2019;**298**:122468. DOI: 10.1016/j.biortech.2019.122468

[22] Lou K, Rajapaksha AU, Ok YS, Chang SX. Pyrolysis temperature and steam activation effects on sorption of phosphate on pine sawdust biochars in aqueous solutions. *Chemical Speciation & Bioavailability*. 2016;**28**:42-50. DOI: 10.1080/09542299.2016.1165080

[23] Plaimart J, Acharya K, Mrozik W, Davenport RJ, Vinitnantharat S, Werner D. Coconut husk biochar amendment enhances nutrient retention by suppressing nitrification in agricultural soil following anaerobic digestate application. *Environmental Pollution*. 2021;**268**:115684. DOI: 10.1016/j.envpol.2020.115684

[24] Guo D, Li Y, Cui B, Hu M, Luo S, Ji B, et al. Natural adsorption of methylene blue by waste fallen leaves of Magnoliaceae and its repeated thermal regeneration for reuse. *Journal of*

- Cleaner Production. 2020;**267**:121903. DOI: 10.1016/j.jclepro.2020.121903
- [25] Hilber I, Bastos AC, Loureiro S, Soja G, Marsz A, Cornelissen G, et al. The different faces of biochar: Contamination risk versus remediation tool. *Journal of Environmental Engineering and Landscape Management*. 2017;**25**:86-104. DOI: 10.3846/16486897.2016.1254089
- [26] Choppala G, Bolan N, Megharaj M, Chen Z, Naidu R. The influence of biochar and black carbon on reduction and bioavailability of chromate in soils. *Journal of Environmental Quality*. 2012; **41**:1175-1184. DOI: 10.2134/jeq2011.0145
- [27] Järup L. Hazards of heavy metal contamination. *British Medical Bulletin*. 2003;**68**:167-182
- [28] Tchounwou PB, Yedjou CG, Patlolla AK, Sutton DJ. Heavy metal toxicity and the environment. *Molecular, Clinical and Environmental Toxicology*. 2012;**101**:133-164. DOI: 10.1093/bmb/ldg032
- [29] Nagajyoti PC, Lee KD, Sreekanth T. Heavy metals, occurrence and toxicity for plants: A review. *Environmental Chemistry Letters*. 2010;**8**:199-216. DOI: 10.1007/s10311-010-0297-8
- [30] Barakat M. New trends in removing heavy metals from industrial wastewater. *Arabian Journal of Chemistry*. 2011;**4**:361-377. DOI: 10.1016/j.arabjc.2010.07.019
- [31] Wuana RA, Okieimen FE. Heavy metals in contaminated soils: A review of sources, chemistry, risks and best available strategies for remediation. *International Scholarly Research Notices*. 2011;**2011**: 1-20. DOI: 10.5402/2011/402647
- [32] Wang Q, Wang B, Lee X, Lehmann J, Gao B. Sorption and desorption of Pb (II) to biochar as affected by oxidation and pH. *Science of the Total Environment*. 2018;**634**: 188-194. DOI: 10.1016/j.scitotenv.2018.03.189
- [33] Paz-Ferreiro J, Lu H, Fu S, Mendez A, Gasco G. Use of phytoremediation and biochar to remediate heavy metal polluted soils: A review. *Solid Earth*. 2014;**5**:65-75. DOI: 10.5194/se-5-65-2014
- [34] Lehmann J, Joseph S. Biochar for environmental management: An introduction. In: Lehmann J, Joseph S, editors. *Biochar for environment management*. 1st ed. Earthscan; 2009. p.1-9
- [35] Inyang M, Gao B, Yao Y, Xue Y, Zimmerman AR, Pullammanappallil P, et al. Removal of heavy metals from aqueous solution by biochars derived from anaerobically digested biomass. *Bioresource Technology*. 2021;**110**:50-56. DOI: 10.1016/j.biortech.2012.01.072
- [36] Wang L, Gao C, Yang K, Sheng Y, Xu J, Zhao Y, et al. Effects of biochar aging in the soil on its mechanical property and performance for soil CO₂ and N₂O emissions. *Science of the Total Environment*. 2021;**782**:146824. DOI: 10.1016/j.scitotenv.2021.146824
- [37] Tan L, Ma Z, Yang K, Cui Q, Wang K, Wang T, et al. Effect of three artificial aging techniques on physicochemical properties and Pb adsorption capacities of different biochars. *Science of the Total Environment*. 2020;**699**:134223. DOI: 10.1016/j.scitotenv.2019.134223
- [38] Xue C, Zhu L, Lei S, Liu M, Hong C, Che L, et al. Lead competition alters the zinc adsorption mechanism on animal-derived biochar. *Science of the Total Environment*. 2020;**713**:136395. DOI: 10.1016/j.scitotenv.2019.136395

- [39] Bai S, Wang L, Ma F, Zhu S, Xiao T, Yu T, et al. Self-assembly biochar colloids mycelial pellet for heavy metal removal from aqueous solution. *Chemosphere*. 2020;**242**:125182. DOI: 10.1016/j.chemosphere.2019.125182
- [40] Yang YQ, Cui MH, Ren YG, Guo JC, Zheng ZY, Liu H. Towards understanding the mechanism of heavy metals immobilization in biochar derived from Co-pyrolysis of sawdust and sewage sludge. *Bulletin of Environmental Contamination and Toxicology*. 2020;**104**:489-496. DOI: 10.1007/s00128-020-02801-4
- [41] Zhang W, Tan X, Gu Y, Liu S, Liu Y, Hu X, et al. Rice waste biochars produced at different pyrolysis temperatures for arsenic and cadmium abatement and detoxification in sediment. *Chemosphere*. 2020;**250**:126268. DOI: 10.1016/j.chemosphere.2020.126268
- [42] Yuan C, Gao B, Peng Y, Gao X, Fan B, Chen Q. A meta-analysis of heavy metal bioavailability response to biochar aging: Importance of soil and biochar properties. *Science of the Total Environment*. 2021;**756**:144058. DOI: 10.1016/j.scitotenv.2020.144058
- [43] Khan ZH, Gao M, Qiu W, Song Z. Properties and adsorption mechanism of magnetic biochar modified with molybdenum disulfide for cadmium in aqueous solution. *Chemosphere*. 2020;**255**:126995. DOI: 10.1016/j.chemosphere.2020.126995
- [44] Teng D, Zhang B, Xu G, Wang B, Mao K, Wang J, et al. Efficient removal of Cd(II) from aqueous solution by pinecone biochar: Sorption performance and governing mechanisms. *Environmental Pollution*. 2020;**265**:115001. DOI: 10.1016/j.envpol.2020.115001
- [45] Zhou Z, Xu Z, Fe NQ, Yao D, Yu J, Wang D, et al. Effect of pyrolysis condition on the adsorption mechanism of lead, cadmium and copper on tobacco stem biochar. *Journal of Cleaner Production*. 2018:996-1005. DOI: 10.1016/j.jclepro.2018.03.268
- [46] Ren X, Sun H, Wang F, Zhang P, Zhu H. Effect of aging in field soil on biochar's properties and its sorption capacity. *Environmental Pollution*. 2018;**2018**(242):1880-1886. DOI: 10.1016/j.envpol.2018.07.078
- [47] Reguyal F, Sarmah AK, Gao WJJOHM. Synthesis of magnetic biochar from pine sawdust via oxidative hydrolysis of FeCl₂ for the removal sulfamethoxazole from aqueous solution. *Journal of Hazardous Materials*. 2017;**321**:868-878. DOI: 10.1016/j.jhazmat.2016.10.006
- [48] Quan G, Fan Q, Cui L, Zimmerman AR, Wang H, Zhu Z, et al. Simulated photocatalytic aging of biochar in soil ecosystem: Insight into organic carbon release, surface physicochemical properties and cadmium sorption. *Environmental Research*. 2020;**183**:109241. DOI: 10.1016/j.envres.2020.109241
- [49] Vithanage M, Rajapaksha AU, Ahmad M, Uchimiya M, Dou X, Alessi DS, et al. Mechanisms of antimony adsorption onto soybean Stover-derived biochar in aqueous solutions. *Journal of Environmental Management*. 2015;**151**:443-449. DOI: 10.1016/j.jenvman.2014.11.005
- [50] Vithanage M, Rajapaksha AU, Ahmad M, Uchimiya M, Dou X, Alessi DS, et al. Mechanisms of antimony adsorption onto soybean Stover-derived biochar in aqueous solutions. *Journal of Environmental Management*. 2015;**2015**(151):443-449. DOI: 10.1016/j.jenvman.2014.11.005

[51] Park JH, Yun JJ, Kang SW, Kim SH, Cho JS, Wang JJ, et al. Removal of potentially toxic metal by biochar derived from rendered solid residue with high content of protein and bone tissue. *Ecotoxicology and Environmental Safety*. 2021;**208**:111690. DOI: 10.1016/j.ecoenv.2020.111690

IntechOpen

IntechOpen